

Article

Investigation of the Fluid Flow in a Large Ball Valve Designed for Natural Gas Pipelines

Laurențiu-Ioan Ivancu [†] and Daniela Popescu ^{*,†} 

Faculty of Machines Manufacturing and Industrial Management, Technical University Gheorghe Asachi of Iasi, B-dul Mangeron nr. 59A, 700050 Iasi, Romania; laurentiu.ioan96@gmail.com

* Correspondence: daniela_popescu@tuiasi.ro; Tel.: +40-746036497

† These authors contributed equally to this work.

Abstract: Natural gas pipeline networks used for long-distance transportation are expanding quickly, and the construction of special valves with large diameters has especially increased since 2022. The design and manufacturing of the flow control equipment is carried out on a case-by-case basis, in accordance with the parameters required by the beneficiary. In this paper, results obtained by fluid flow simulation with SolidWorks2023 software for a 500 mm diameter trunnion ball valve lead to important information regarding how the fluid flow develops in the intermediary and fully closed positions. The large inner space of the ball allows the development of high-amplitude vortices; thus, the simulation demonstrates that the shut-on/off operation of large-diameter ball valves is mandatory to avoid fast destruction following partial opening. This paper also demonstrates why the metal–metal (MM) sealing with a double-piston effect (DPE) design for seats produces low leakage rates, including for the shut-off position; the pressure field reveals that few gas particles succeed in crossing the upstream sealing zone, and even fewer cross the downstream sealing zone. Additionally, the interpretation of the results explains and highlights the importance of using seats with a DPE design to achieve fire safety, which is required for natural gas pipeline applications.

Keywords: trunnion ball valve; double-piston effect; valve seat; SolidWorks fluid flow simulation; natural gas pipelines; Repower EU Plan



Citation: Ivancu, L.-I.; Popescu, D. Investigation of the Fluid Flow in a Large Ball Valve Designed for Natural Gas Pipelines. *Appl. Sci.* **2023**, *13*, 4247. <https://doi.org/10.3390/app13074247>

Academic Editor: Satoru Okamoto

Received: 5 February 2023

Revised: 20 March 2023

Accepted: 22 March 2023

Published: 27 March 2023



Copyright: © 2023 by the authors. Licensee MDPI, Basel, Switzerland. This article is an open access article distributed under the terms and conditions of the Creative Commons Attribution (CC BY) license (<https://creativecommons.org/licenses/by/4.0/>).

1. Introduction

The natural gas demand in the EU reached 15,834,900 terajoules in 2021 [1]. Gas represents 21.5% of the EU's primary energy consumption and covers 32.1% of energy demand for households. The EU gas network contains more than 200,000 km of transportation pipelines and over 2 million km of distribution networks [2]. In 2022, following the invasion of Ukraine, new natural gas transportation pipelines—such as the interconnectors Greece–Bulgaria, Poland–Slovakia, and Romania–Moldovia—aimed to contribute to the security of the gas supply in Central and Eastern Europe [3].

To be in line with the objectives set out in the Repower EU Plan [4], companies specialized in the production of valves for the gas and oil industry must identify the best solutions for large valves, which have to be constructed to answer the specific requirements on a case-by-case basis. The uniqueness of the design for large valves is the result of a combination of factors, such as the underground or the on-ground location, the climate framework (which can expose them to extreme weather), the composition of the natural gas, the physicochemical composition of the soil, and disaster conditions, such as fire development in the pipeline or heavy floods. Additionally, high pressure and large diameters lead to higher stress for components, and the risk of destruction can be significant during dynamic operation. The mechanical engineer has to propose a holistic solution to answer to all of these challenges, as well as the special requirements of beneficiaries. For instance, the standard recommends the use of the steel type A350 LF2 for the bodies of valves and

for the metal sealing components (i.e., the ball and the seats) of ball valves implemented in natural gas pipelines [5], but when the soil surrounding the underground pipeline contains salty hydrocarbons, the beneficiaries prefer stainless steel as the material.

In the natural gas industry, a lot of categories of valves are used, including ball valves [6], check valves [7], plug valves [8], float valves [9], gate valves [10], and butterfly valves [11]. Safe operation is very important for natural gas transportation, and in this context, an appropriate design for the shut-off of large-diameter ball valves is crucial. The scientific literature proposes a wide range of methods to be used for research in this domain. Computational fluid dynamics (CFD) can be used to obtain important information based on the analysis of the fluid flow in small or medium-sized ball valves by simulation.

Jia, M. et al. investigated four different V-sector valve core opening shapes to be used in a DN65 ball valve. The best solution, designed to work with hot water in a secondary heating system, was identified by using ANSYS [12].

Yu, R. et al. proposed an innovative elastic valve seat for V-shaped ball valves, composed of a blade spring coil, a support back ring, and a sealing ring, adequate for powders or other media with granular matter. Mud with particulate matter was selected as the medium. The results of their study, based on fluid dynamics simulation with SolidWorks 2021 software and experiments on DN50, DN65, DN80, DN100, and DN125 ball valves, showed that the fatigue strength of the ball spool and the spring-loaded plate seat structure enabled the valve to comply with high safety standards. This highly efficient sealing is possible because it avoids the problem of sealing failure caused by granular media entering the spring cavity, or by the valve seat bonding on the valve body [13].

Song, X. et al. used the finite element method to study the construction of a ball valve made of CF8M stainless steel. The purpose was to optimize the mass and the structural safety of the ball valve, with the target being an accurate flow coefficient. The analysis was carried out for seven opening positions of the ball: 0°, 15°, 20°, 30°, 50°, 70°, and 90°. By optimization using an orthogonal array, the response surface method and trade-off method demonstrated that the weight could be reduced by up to 16.67% (from 2.34 to 1.95 kg) for the studied balls, which had radii of 37/35/33 mm. The results highlight that when using ASTM A296 CF8M as the construction material, the ball valve was more resistant to corrosion and provided higher strength at different temperatures, compared to balls made from CF8 [14].

The particle tracking flow visualization (PTFV) method can also be used to determine flow characteristics and flow patterns. Chern M. et al. performed an experimental study on a DN50 ball valve to observe the flow patterns for different opening angles and cavity phenomena [15]. The study concluded that such a method represents an effective way to determine the performance coefficients of a valve and to understand how and when cavitation can occur.

Cui, B. et al. studied the evolution of flow characteristics for different openings using FLUENT. They observed how a DN50 ball valve opening or closing within different time intervals developed different fluid flow patterns. If the opening/closing period is long, the flow rate, the inlet and outlet pressure, the pressure drop, and the flow resistance are similar to the steady condition. These results can offer support for increasing the dynamic performance during the opening and closing process [16].

Peng, C. et al. conducted a comparative analysis on two types of metallic seats for ball valves: one with the multi-asperity model and one with the magnification-based model. The scope was to study leakage simulation for a ball valve, using water as the working fluid. Simulations performed by ANSYS and experiments on a ball with a radius of 20 mm were performed. The best simulation results were obtained for the magnification model, which was the one that provided the best match to the experimental results [17].

The works [12–17] focus on new valves. Some researchers were more interested in the phenomena that occur in the components of old pipelines. For instance, Velázquez, J. et al. studied the failure pressure in aged pipelines using the finite element method, considering

the changes in mechanical characteristics following a long working period. Their results demonstrated that corrosion defects and aging have an impact on the failure pressure [18].

In contrast to previously presented works that focused on ball valves of up to 125 mm in diameter, the present study focuses on CFD simulation of the fluid flow in a large ball valve. A trunnion ball valve with a diameter of 500 mm, with metal–metal (MM) sealing and double-piston effect (DPE) seats, is the type of valve analyzed in the present work. This paper aims to contribute to the research field by studying the behavior during the closing process of a sealing technology recommended for ball valves with components, materials, and technologies selected to answer to the challenges of natural gas transportation within the large-diameter domain. The investigated valve was designed according to the standard API 6D [19] and the corresponding European standard SR EN ISO 14313 [20], which are the standards that specify requirements and provides recommendations for the design, manufacturing, testing, and documentation of ball, check, gate, and plug valves for application in pipeline systems meeting the requirements for the petroleum and natural gas industries. The simulation was performed using SolidWorks Fluid Flow 2023 software.

The main originality of this paper consists in the simulation of a large-diameter ball valve working at a high class of pressure (Class 400), as well as providing explanations about why MM sealing with a DPE design for seats is appropriate to obtain high valve safety by limiting leakages. To the best of our knowledge, this topic has not been the focus of other works.

Ball valves are shut-off valves, designed to work at 0° and 90° opening positions. A large-diameter ball valve can withstand high forces that develop as a consequence of the difference between the momentum before and after opening/closing. Moreover, the acting moment is high, the actuator needs time to perform the stroke, and the opening time can be at least 40 s. Different phenomena might occur during the process; therefore, to highlight the correlation between the changes in the fluid flow motion and the changes in the configuration of the solid walls that represent the boundaries of the fluid flow simulation domain, five case studies representing different positions of the ball—30°, 45°, 60°, 70°, and fully closed (90°)—were studied. The validation of the results presented in Section 4 consisted of experimental tests on a ball valve with a 500 mm diameter and metal–metal sealing with a DPE design, similar to the digital twin model analyzed by the simulations. The results of the experimental tests confirm the high quality of the sealing that was determined and explained by analyzing the fluid flow using SolidWorks software.

In the present work, the trajectories, pressure, and velocity fields inside the DN500 ball valve were studied. The scope of this article is to investigate the movement of the fluid, with a special focus on the sealing zones of the seats, where the impact of the high pressure can be significant. This paper demonstrates how the sealing zone of the seats—especially the upstream sealing seat—is most vulnerable to rapid destruction. Our results can be applied to identify adequate solutions to increase the reliability of the entire valve.

This paper is organized as follows: In the first section, the importance and the actuality of the topic is introduced, and the scientific literature review is discussed. In Section 2, the methodology is described. Section 3 contains the presentation and interpretation of the results obtained using SolidWorks Flow Simulation 2023. Section 4 presents the experimental tests. The final section concludes on the effects specific to the fluid movement inside a large-diameter ball valve working with natural gas at high pressure (6.3 MPa).

2. Methods

Metal–metal sealing is well known to be one of the safest methods, and according to API6D and ISO 14313 this type experiences very little leakage [19,20].

According to the standard SR EN 3317:2015, the composition of the natural gas is at least 85% methane (CH₄), and the remaining 15% is composed of the major components ethane (C₂H₆), propane (C₃H₈), butane (C₄H₁₀), pentane (C₅H₁₂), hexane (C₆H₁₄), nitrogen (N₂), and carbon dioxide (CO₂), and the minor components hydrogen (H₂), oxygen (O₂), carbon monoxide (CO), and helium (He) [21]. In the studied case, a density of 0.717 kg/m³

was taken into consideration for the simulation—a value calculated for the previous composition, which is in accordance with the standard and with the Romanian Energy Regulatory Authority (ANRE) regulations [22]. For this fluid, the critical temperature is 190.56 K, the critical pressure is 4,599,200 Pa, and the critical compressibility factor is 0.286243.

The principal components of the ball valve are the ball, the principal body, the upstream secondary body, the downstream secondary body, two identical seats, the acting stem, two identical guiding plates, and the connecting piece (see Figure 1). The studied valve was a trunnion type, which differs from other categories by virtue of the fact that the ball is held firmly by two guiding plates.

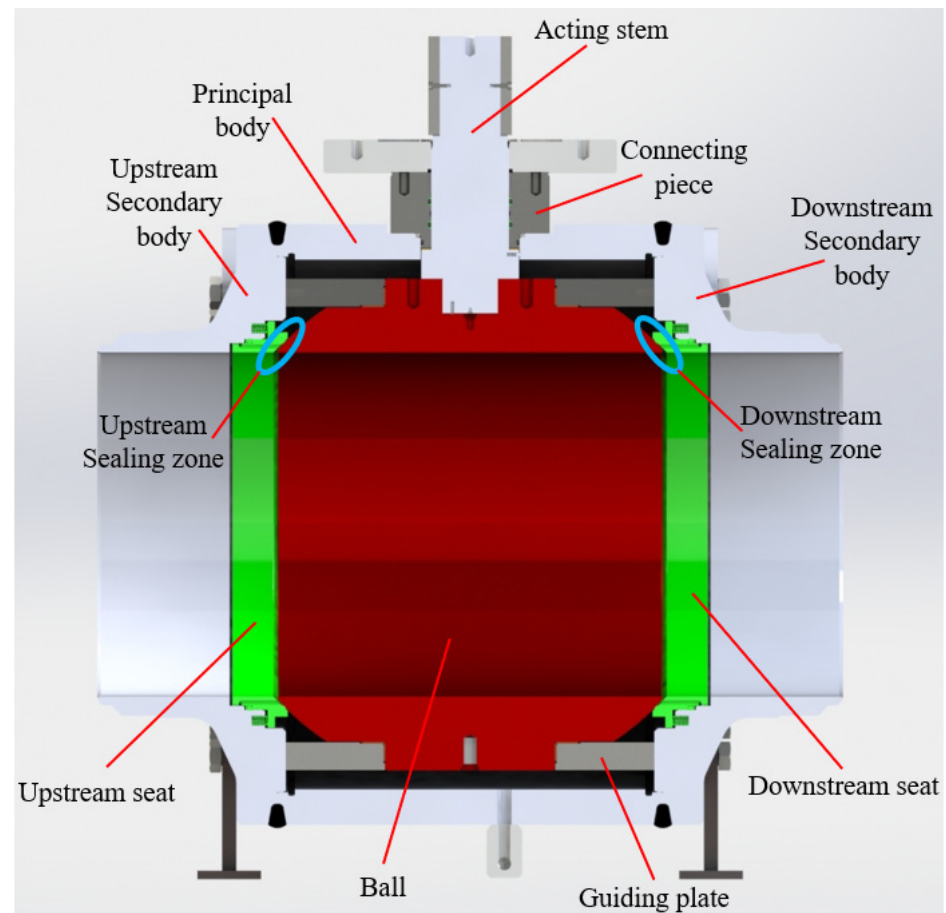


Figure 1. Ball valve components (front section).

The closing of the ball valve takes place as follows: when the fluid flow moves from upstream to the closed valve, the upstream seat is pushed on the ball by the pressure through the gasket and by the springs; in that moment, the metal sealing surface from the seat covered with tungsten carbide is in contact with the metal sealing surface from the ball (also covered with tungsten carbide), and the sealing is completed. Tungsten carbide has several important advantages, including high strength, high resistance, high precision, good temperature resistance, and good corrosion resistance [23]. The producers of balls and seats coated with tungsten carbide claim that the coated balls and seats keep their high sealing qualities after more than 70,000 cycles [24].

The sealing of seats using the DPE design solution can provide highly efficient sealing, due to the two O-ring gaskets situated at two stages to ensure the same sealing performance upstream and downstream. Other sealing construction designs, such as the SPE (single-piston effect), provide efficient sealing only from the outside to the inside of the valve [25].

The case studies analyzed using SolidWorks Flow Simulation 2023 are presented in Section 3. One hypothesis assumed for the simulations was that the ball valve was

constructed from rigid elements, which would mean that there were no deformations of the shape generated by compression. The defined boundary conditions were as follows: at the inlet section (upstream), the nominal pressure was 6.3 MPa and the velocity was 20 m/s; at the outlet section (downstream), the pressure was atmospheric pressure and the velocity was 0 m/s. SolidWorks Flow Simulation employs transport equations for the turbulent kinetic energy and the $k - \epsilon$ model for the dissipation rate.

To provide more robust and accurate simulations, nested iterations are used by the SolidWorks solver to allow treatment of the mutual influence of flow parameters and boundary conditions. These iterations are run step by step and repeated until the solver convergence is obtained, a maximum number of nested iterations is reached, or each conservation law's convergence condition is satisfied. The convergence solver allows that identification of the goals that converge, in contrast to those that do not converge or have no solution [26]. SolidWorks Flow Simulation solves the mass, momentum, and energy conservation laws for fluid flows, fluid state equations, and the empirical dependencies of fluid density, viscosity, and thermal conductivity on temperature. The conservation laws for mass, angular momentum, and energy, along with the additional equations necessary to describe the fluid motion, are presented below as Equations (1)–(16), which were extracted from the manual of the SolidWorks software [26].

$$\frac{\partial \rho}{\partial t} + \frac{\partial}{\partial x_i}(\rho u_i) = S_M^p \tag{1}$$

$$\frac{\partial \rho u_i}{\partial t} + \frac{\partial}{\partial x_i}(\rho u_i u_j) + \frac{\partial p}{\partial x_i} = \frac{\partial}{\partial x_j}(\tau_{ij} + \tau_{ij}^R) + S_i + S_{I_i}^p, \quad i = 1, 2, 3; j = 1, 2, 3 \tag{2}$$

$$\frac{\partial \rho H}{\partial t} + \frac{\partial \rho u_i H}{\partial x_i} = \frac{\partial}{\partial x_i} [u_j (\tau_{ij} + \tau_{ij}^R) + q_i] + \frac{\partial \rho}{\partial t} + S_i u_i + S_H^p + Q_H \tag{3}$$

$$H = h(P, T, y) + \frac{u^2}{2} + k \tag{4}$$

where u is the fluid velocity, ρ is the fluid density, and S_i is a mass-distributed external force per unit mass due to the porous media's resistance (S_i^{porous}), gravity ($S_i^{gravity} = \rho g_i$, where g_i is the gravitational acceleration component along the i -th coordinate direction), and the coordinate system's rotation ($S_i^{rotation}$).

$$S_i = S_i^{porous} + S_i^{gravity} + S_i^{rotation} \tag{5}$$

H is the total enthalpy in the local reference frame; $h(P, T, y)$ is the thermal enthalpy at a given pressure (P), temperature (T), and fluid mixture components y ; $y = (y_1 \dots y_n)$ is the concentration vector of the fluid mixture components; k is the kinetic energy of turbulence; S_M^p , $S_{I_i}^p$, and S_H^p are additional interfacial exchange terms due to Euler-Lagrange particle interaction; Q_H is the heat source or sink per unit volume; τ_{ij} is the viscous shear stress tensor; q_i is the diffusive heat flux.

The energy equation for calculation with a high Mach number flow is as follows:

$$\frac{\partial \rho E}{\partial t} + \frac{\partial \rho u_i (E + \frac{p}{\rho})}{\partial x_i} = \frac{\partial}{\partial x_i} [u_j (\tau_{ij} + \tau_{ij}^R) + q_i] - \tau_{ij}^R \frac{\partial u_i}{\partial x_j} + \rho \epsilon + Q_H \tag{6}$$

$$E = e(\rho, T, y) + \frac{u^2}{2} \tag{7}$$

where $e(\rho, T, y)$ is the integral energy at a given fluid density (ρ), temperature (T), and fluid mixture components y .

The viscous shear stress tensor for Newtonian fluids is as follows:

$$\tau_{ij} = \mu \left(\frac{\partial u_i}{\partial x_j} + \frac{\partial u_j}{\partial x_i} - \frac{2}{3} \delta_{ij} \frac{\partial u_k}{\partial x_k} \right) \tag{8}$$

The Reynolds stress tensor according to the Boussinesq assumption is as follows:

$$\tau_{ij}^R = \mu_t \left(\frac{\partial u_i}{\partial x_j} + \frac{\partial u_j}{\partial x_i} - \frac{2}{3} \delta_{ij} \frac{\partial u_k}{\partial x_k} \right) - \frac{2}{3} \rho k \delta_{ij} \tag{9}$$

where δ_{ij} is the Kronecker delta function, μ is the dynamic viscosity, μ_t is the turbulent eddy viscosity coefficient, and k is the turbulent kinetic energy.

Two additional transport equations are used to describe the turbulent kinetic energy (k) and the dissipation (ϵ) :

$$\frac{\partial \rho k}{\partial t} + \frac{\partial}{\partial x_i} (\rho u_i k) = \frac{\partial}{\partial x_i} \left(\left(\mu + \frac{\mu_t}{\sigma_k} \right) \frac{\partial k}{\partial x_i} \right) + S_k \tag{10}$$

$$\frac{\partial \rho \epsilon}{\partial t} + \frac{\partial}{\partial x_i} (\rho u_i \epsilon) = \frac{\partial}{\partial x_i} \left(\left(\mu + \frac{\mu_t}{\sigma_\epsilon} \right) \frac{\partial \epsilon}{\partial x_i} \right) + S_\epsilon \tag{11}$$

where S_k and S_ϵ are defined as follows:

$$S_k = \tau_{ij}^R \frac{\partial u_i}{\partial x_j} - \rho \epsilon + \mu_t P_B \tag{12}$$

$$S_\epsilon = C_{\epsilon 1} \frac{\epsilon}{k} \left(f_1 \tau_{ij}^R \frac{\partial u_i}{\partial x_j} + \mu_t C_B P_B \right) - C_{\epsilon 2} f_2 \frac{\rho \epsilon^2}{k} \tag{13}$$

P_B is the turbulent generation due to buoyancy forces:

$$P_B = - \frac{g_i}{\sigma_B} \frac{1}{\rho} \frac{\partial \rho}{\partial x_i} \tag{14}$$

where g_i is the component of gravitational acceleration in direction x_i , the constant $\sigma_B = 0.9$, and the constant C_B is defined as follows: $C_B = 1$ when $P_B > 0$, and 0 otherwise.

$$f_1 = 1 + \left(\frac{0.05}{f_\mu} \right)^3, \quad f_2 = 1 - \exp(-R_T^2) \tag{15}$$

The constants C_μ , $C_{\epsilon 1}$, $C_{\epsilon 2}$, σ_k , and σ_ϵ are defined empirically; SolidWorks Flow Simulation uses the following typical values:

$$C_\mu = 0.09, \quad C_{\epsilon 1} = 1.44, \quad C_{\epsilon 2} = 1.92, \quad \sigma_k = 1, \quad \sigma_\epsilon = 1.3 \tag{16}$$

The computational domain is limited by the inlet section, the outlet section, and the lateral area in the vicinity of the walls. The methodology that defines the discretization network, named mesh, is the same for all case studies, while the position of the ball towards the longitudinal axis of the valve causes the internal zone delimited by the walls to be different. Since the diameter of the valve is large, the mesh must contain many nodes to describe the large computational domain; the total number of cells is 4,769,616, and the number of fluid cells in contact with the solid walls is 2,425,418. To ensure the best results, the refinement of the mesh was accentuated in the most important areas—the inlet and the outlet sealing zones situated in the vicinity of the seats and of the ball, and also at the internal walls of both secondary bodies. Details are presented in Figure 2.

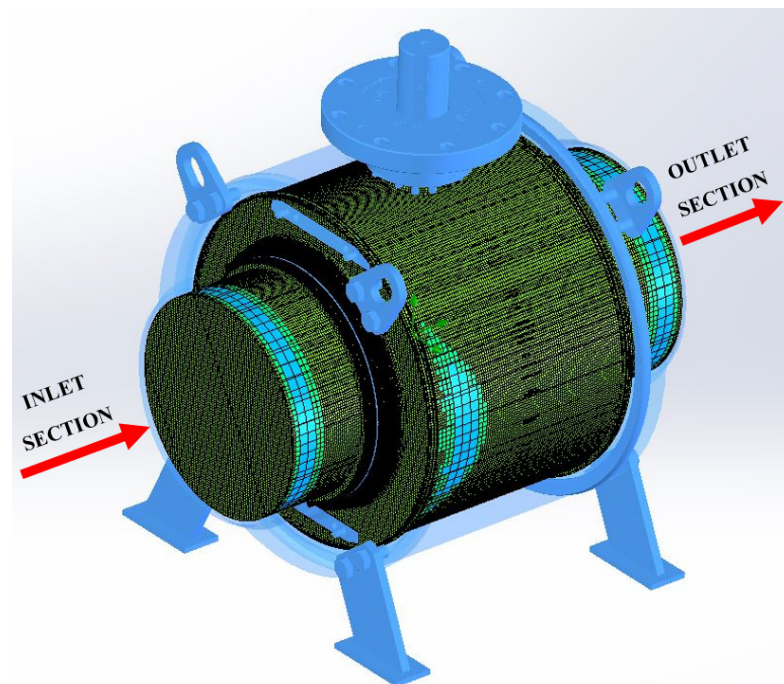


Figure 2. General view of the mesh (discretization network).

The first four case studies consisted of research on the fluid motion inside the ball valve at different closure angles (30° , 45° , 60° , and 70°), and the last case study focused on the fully closed ball valve situation, defined as a 90° closure angle.

The dependence between the flow factor Kv and the closure angle, as presented in Figure 3, indicated that for each angle of closure there were significant differences in the values of Kv [27]. The simulation and interpretation of the results presented in the following section provide interesting explanations.

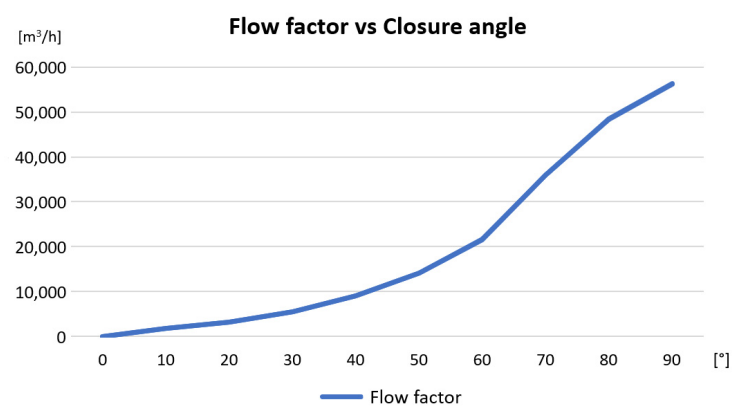


Figure 3. Flow factor according to closure angle for a DN500 ball valve.

3. Results and Discussion

3.1. 30° Closure Angle

The fluid dynamics of a DN500 ball valve was first studied for a 30° angle between the longitudinal axis of the pipe/ball valve and the longitudinal axis of the ball. The pressure losses are so small for lower closing angles that there is no purpose in studying the fluid dynamics inside the valve, since it suffers only slight deviations compared to the fully open situation. If the ball valve is fully opened, the fluid flow is almost the same as in the pipe, because the ball is designed to have an adequate shape.

For a closure angle of 30° , the gas with 6.3 MPa upstream pressure crosses the ball valve without being significantly diverted by large obstacles, because the opening is large.

In Figure 4, the first loss of pressure can be observed after the upstream sealing zone, because here the section is narrow. The second loss, which reduces the pressure to almost 6.2 MPa, can be observed in the downstream sealing zone. In this situation, the pressure drop is low, but the use of the valve in this position for an extended period can cause damage. The explanation for this is that the mixture of the gas and impurities—indicated in Figure 4a by the purple color—strikes a small surface of the upstream sealing zone and can peel off the coated layer of tungsten carbide, similar to a sanding process.

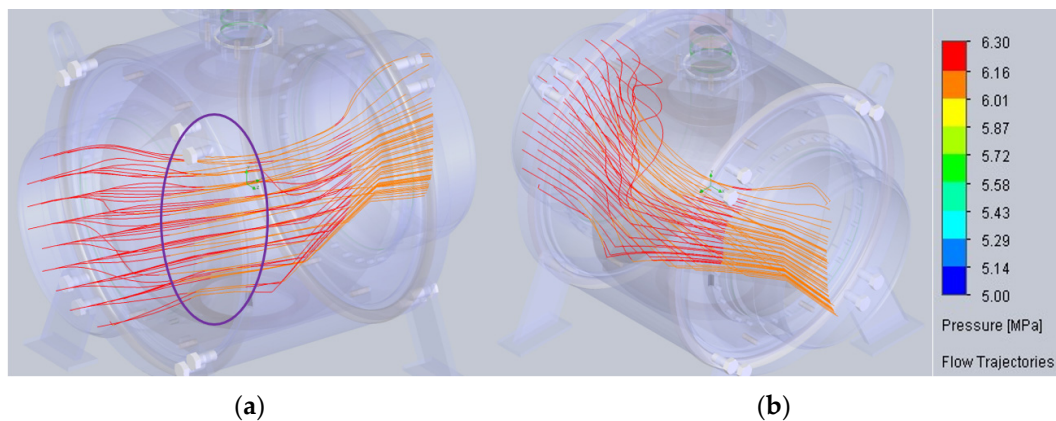


Figure 4. Pressure line trajectories for a 30° closure angle: (a) upstream view; (b) downstream view.

Figure 5 indicates that for this opening, the velocity that was 20 m/s in the inlet section becomes 50 m/s in the ball cavity, situated between the first sealing zone and the second sealing zone. Two small vortices are trying to develop—one at the upstream sealing zone and the other one at the downstream sealing zone. However, their amplitude is very small, and the vortices dissipate quickly without having any significant impact on the main stream and, consequently, on the movement of the fluid inside the ball valve. The maximum velocity is low—not very different to the velocity in the fully open position, because there is enough space for the movement of the fluid.

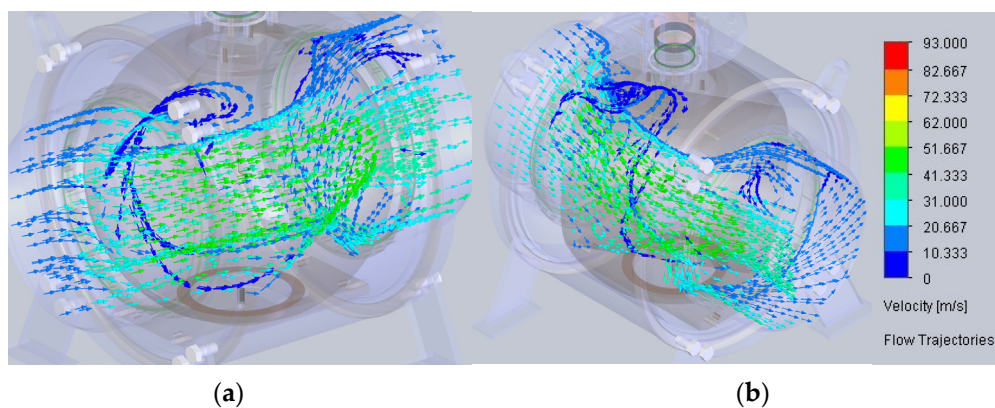


Figure 5. Velocity line trajectories for a 30° closure angle: (a) upstream view; (b) downstream view.

3.2. 45° Closure Angle

In this case, the methane enters the internal cavity of the secondary body of the ball valve from the upstream pipe and tries to disperse inside the entire valve.

As can be observed in Figure 6, the gas hits the sealing surface between the sealing seat and the ball, i.e., the so-called upstream sealing zone. In this area, chaotic movement of particles starts, and the first local loss of pressure from 6.3 MPa to 6.15 MPa can be observed. The trajectories deviate downstream because the gas has to pass through the sealing area to enter the cavity of the ball. This is the second zone where the pressure decreases; the

pressure changes from 6.15 MPa to 5.9 MPa, the agitation phenomenon begins, and vortices are generated. Downstream, the gas particles regroup and are further driven by the main fluid flow to leave the cavity of the ball through the downstream secondary body, with a pressure of 5.9 MPa.

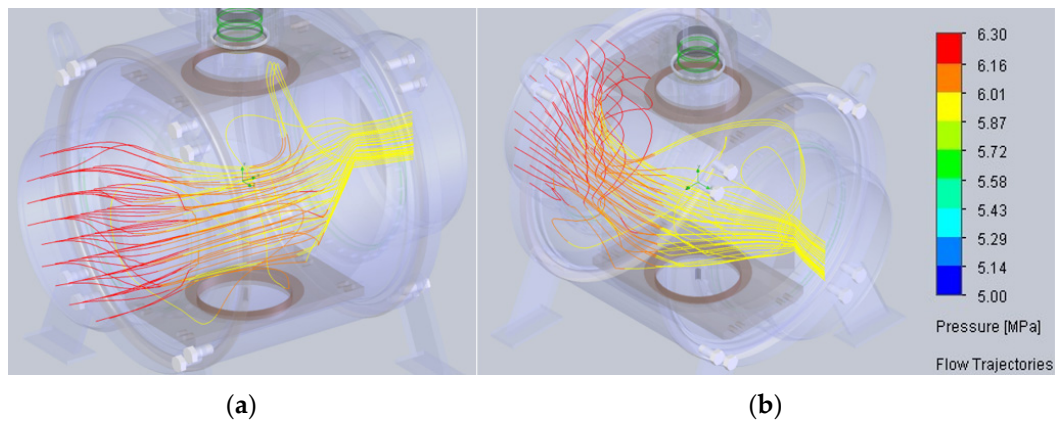


Figure 6. Pressure line trajectories for a 45° closure angle: (a) upstream view; (b) downstream view.

The velocity line trajectories presented in Figure 7 show that the first modification of velocity from 20 m/s upstream in the pipe can be noticed at the upstream sealing zone, when the fluid starts to show chaotic movement. The gas hits the ball and the sealing surface at a velocity of almost 40 m/s. The highest velocity rate is reached in the cavity of the valve, where the agitation phenomenon of the gas particles leads to it reaching almost 90 m/s. The different trajectories and rates of velocity in the internal area of the ball and in the superior and inferior extremities of the internal wall are caused by the external geometry of the ball. The gas has the highest velocity in the cavity of the ball (yellow and orange color) and the lowest at the extremities (blue color). The pressure decreases, and the generation of the vortex determines the increase in the energy loss, both because of the size and because of the deviation in the trajectories due to the position of the valve. If the ball valve is used at a 45° closure angle, the pipe system needs more energy to maintain the same volumetric flow rate, because of the restricted valve opening. The greatest negative impact can be observed on the upstream seat, because the gas particles—which can contain some impurities in their composition—hit the surface of the sealing seat violently. The area of contact between the seat and the surface of the ball, denoted as A in Figure 7, is vulnerable to rapid destruction. The result is the separation of the coating material of the seat (i.e., the tungsten carbide).

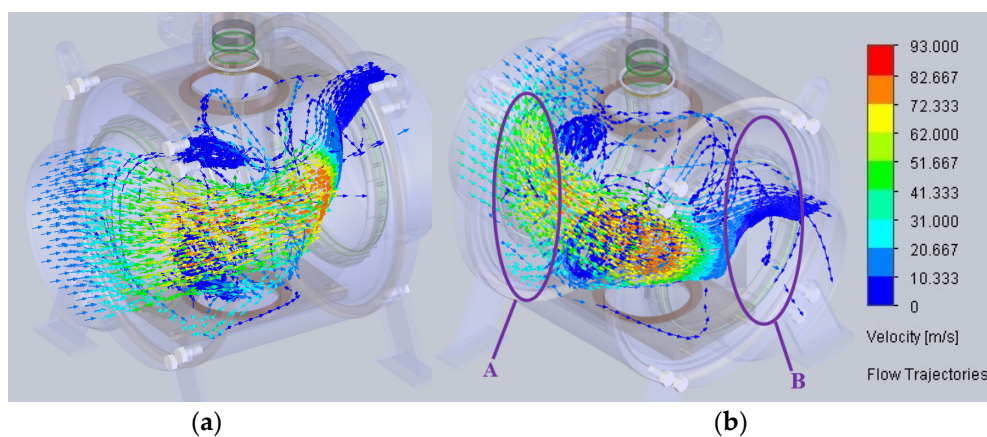


Figure 7. Velocity line trajectories for a 45° closure angle: (a) upstream view; (b) downstream view.

Moreover, it may be observed that not all of the particles have the same velocity—some of them keep moving at 20 m/s. Once they leave the turbulent zone containing a vortex, the velocity decreases to 10–15 m/s. In the zone denoted as B in Figure 7, the gas hits half of the downstream sealing seat and a part of the internal cavity of the ball, making this seat also vulnerable to rapid destruction. The vortex size can be estimated by comparison to the dimensions of the ball. Some vortices can fill almost all of the internal zone of the ball, meaning that perturbations are important and local energy losses are significant. According to Ming-Jyh Chern et al., “In general, the inlet velocity and the valve opening play very important roles to the performance of a ball valve” [15]. Downstream of the valve, the velocity stabilizes at a rate of 20 m/s—the same as the upstream velocity in the pipe.

3.3. 60° Closure Angle

If the closing process continues, the turbulence phenomenon becomes more intense.

The upstream pressure of 6.3 MPa decreases to 6.1 MPa at the entrance in the cavity of the ball, because the area is more restricted by the new position of the ball. In this area, the first stage of pressure losses develops. The second stage is due to the vortex, when the gas particles try to regroup and the pressure rates are in the range of 5.4 to 6 MPa. The gas leaves the ball cavity at a stabilized pressure of 5.4 MPa, observed in this zone and also at the second sealing section, as depicted in Figure 8.

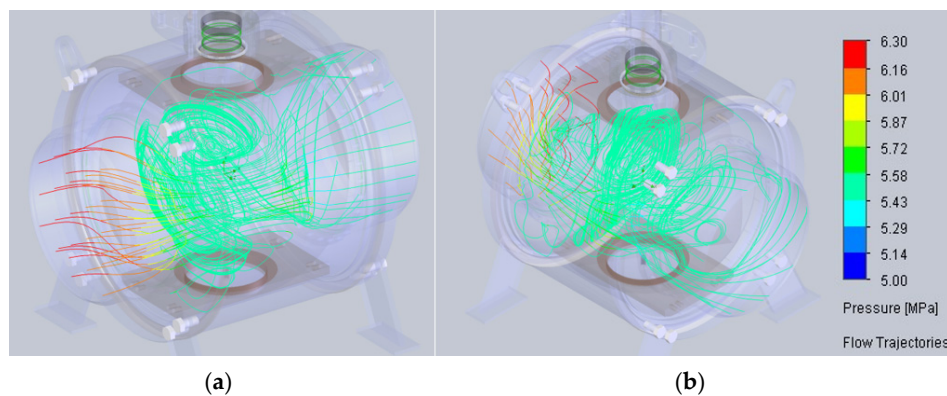


Figure 8. Pressure line trajectories for a 60° closure angle: (a) upstream view; (b) downstream view.

Figure 9 indicates that the initial gas velocity is amplified in the zone where the first loss of pressure occurs, reaching almost 55 m/s. Some gas particles enter the cavity by passing between the internal wall of the principal body and the external wall of the ball, at low fluid flow rates of around 10 m/s. This happens because the quantity of the flow crossing the ball cavity is relatively high. In the vortex area, a velocity of 95 m/s is reached. The circulation of gas through the downstream secondary body takes place at 20 m/s, except for some trajectories. Downstream, the velocity becomes steady in the pipe.

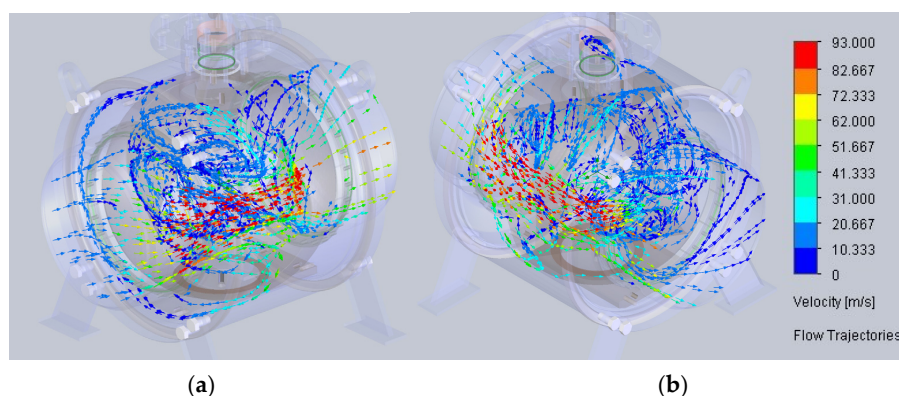


Figure 9. Velocity line trajectories for a 60° closure angle: (a) upstream view; (b) downstream view.

3.4. 70° Closure Angle

The action of the fluid on a large area of the external surface of the ball generates a significant loss of energy. For a DN500 type ball valve, in this position, the flow factor is $K_v = 35,984$ [27].

Figure 10 indicates that the nominal pressure is 6.3 MPa (red color) and the initial velocity of the methane is 20 m/s upstream of the ball valve, which is slightly open. The pressure decreases abruptly to almost 5 MPa in the upstream sealing zone, except for several trajectories. It may be observed that only some fluid flow particles, with 5.2 to 6 MPa pressure, manage to enter the internal zone of the ball without significant modification of the upstream trajectories. In the internal zone of the ball, a large vortex develops. The fluid tries to leave the zone by passing through the small 20° opening, after regrouping in a more ordered way, but some particles pass between the seats and the ball, as can be observed in the area denoted as A. In the outlet section, the pressure is almost 5 MPa (dark blue color).

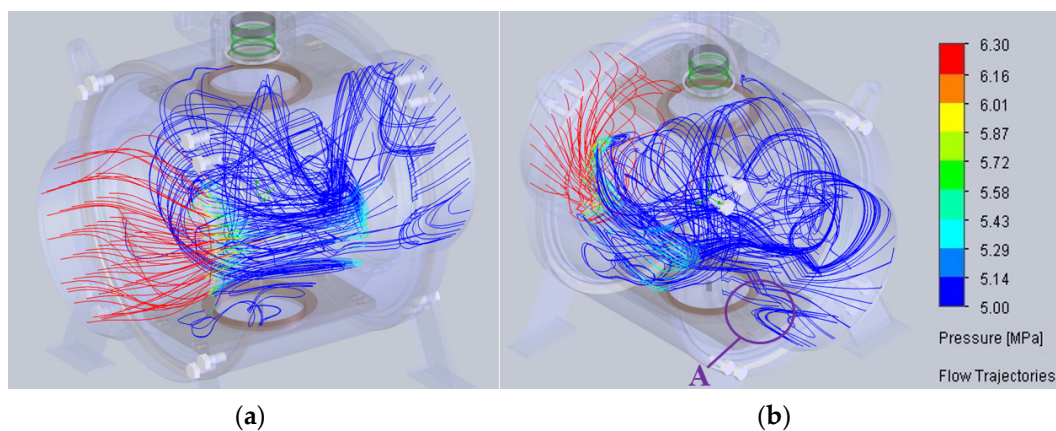


Figure 10. Pressure line trajectories for a 70° closure angle: (a) upstream view; (b) downstream view.

According to the simulation results presented in Figure 11, the velocity is amplified to almost 95 m/s by the small entrance area in the internal zone of the ball (red color). In the vortex area, this high rate of velocity is conserved, but outside of it some particles decelerate. The exit from the internal zone of the ball is crossed by particles with different velocities in the second sealing zone, in the range of 20–50 m/s. At the exit of the downstream secondary body, the velocity is close to the initial value, i.e., 20 m/s.

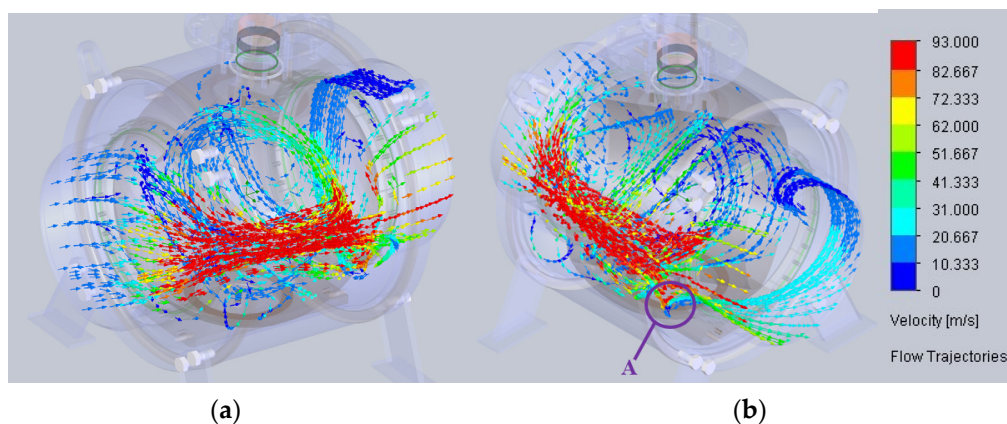


Figure 11. Velocity line trajectories for a 70° closure angle: (a) upstream view; (b) downstream view.

3.5. 90° Closure Angle

In Figure 12, the computational domain is presented for the 90° closure angle position.

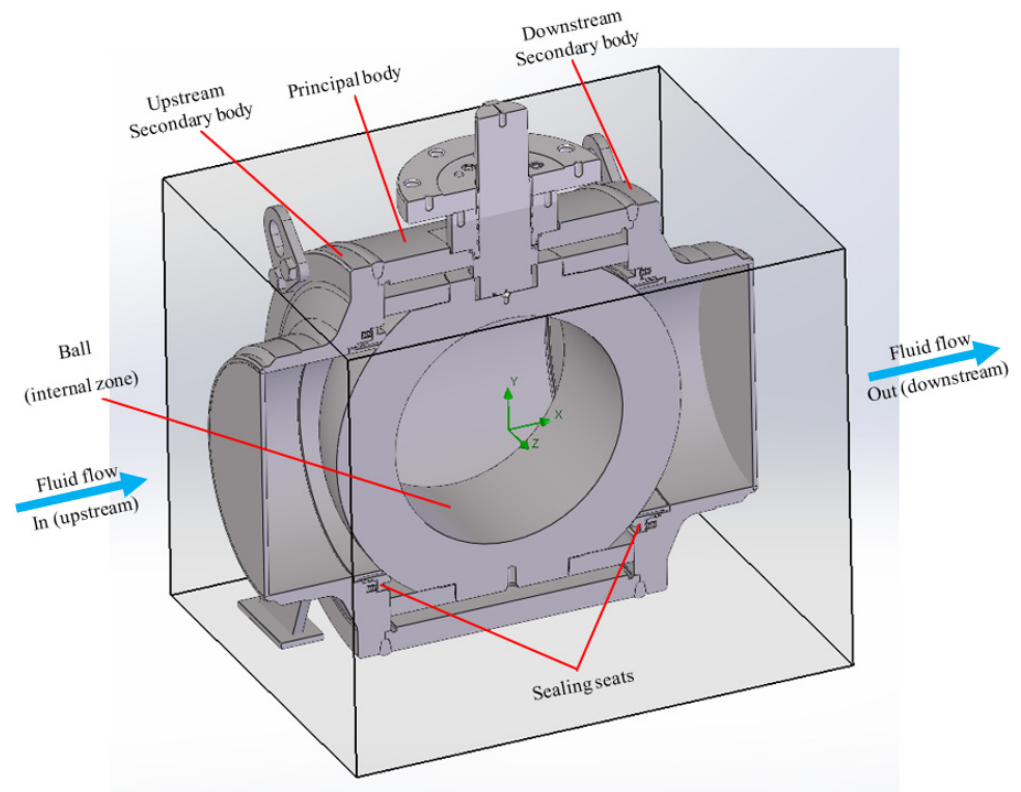


Figure 12. Computational domain of the ball valve in the 90° closure angle position.

The analysis focuses mainly on the internal area of the ball valve. Results concerning the pressure field are presented for the fully closed valve. In Figure 13, it may be observed that the 6.3 MPa pressure (red), corresponding to 20 m/s velocity upstream, is distributed on the entire circular body almost equidistantly in the inlet zone. The first modification occurs at the contact zone between the upstream and downstream sealing zones (yellow, green, and light blue). It may be observed that the pressure is $p \approx 2$ MPa (light blue) in the internal zone of the ball. This pressure exists because the metal–metal sealing does not assure 100% contour contact, and some particles are able to pass. In the downstream sealing zone, the pressure decreases significantly, and a small pressure contour (blue) with a nominal pressure of around 1 MPa is visible in the area situated between the end of the downstream seat and the beginning of the internal circular surface of the secondary body, as shown in Figure 13b.

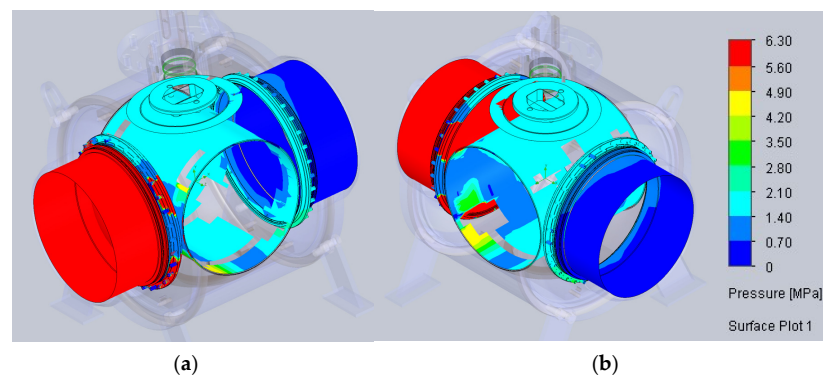


Figure 13. Pressure contour for the fully closed valve: (a) upstream view; (b) downstream view.

This is the consequence of the double-piston effect (DPE). Therefore, if the sealing seat construction had been of the SPE type, the leakages of this ball valve would be expected to be similar to those obtained in the internal area of the ball for the DPE type ($p \approx 2$ MPa). In

conclusion, the fact that there is a pressure contour on the internal wall of the secondary body does not mean that the leakage is important. On the contrary, only a very small quantity of gas particles can pass, and the pressure is lower and well distributed on the internal wall of the secondary body. Downstream of the valve, in the pipe, the low number of gas particles has no impact on the pressure distribution.

Figure 14 presents the trajectories of the gas particles, including pressure information. The methane enters with a pressure of 6.3 MPa from the pipe and hits the body of the valve, which dissipates it. A small quantity of the fluid flow, represented by yellow (4.2 to 4.9 MPa), green (2.8 to 4.2 MPa), and light blue (0.7 to 2.8 MPa) arrows, passes between the sealing seat and the ball (the so-called upstream sealing zone). In the area between the upstream sealing zone and the downstream sealing zone, the fluid develops low pressure, depicted in dark blue (up to 0.7 MPa). This pressure has impact on the internal wall of the principal body and generates vortices before the second sealing zone.

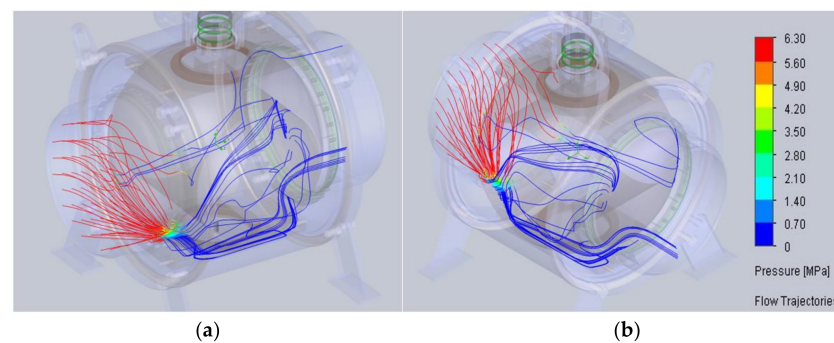


Figure 14. Fluid flow trajectories for the fully closed valve: (a) upstream view; (b) downstream view.

In this work, the distance between the internal wall of the principal body and the external wall of the ball (the gap) taken into consideration is 7 mm (see Figure 15). Such a value is not a standard dimension; the manufacturer decides which is the best rate based on the construction technology used for the ball and the principal body. The purpose of the gap is to avoid blockages within the operation of the ball valve at different openings.

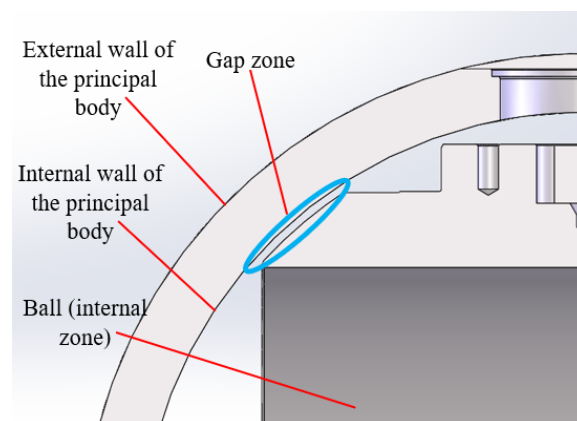


Figure 15. Gap between the principal body and the DN500 ball.

The pressure in the internal area of the valve is higher than the atmospheric pressure, indicating that the metal–metal sealing leads to a situation where there is fluid in the space situated between the internal wall of the principal body and the sealing seats. Although this is not the ideal situation, the issue can be solved by applying the DPE design solution on the sealing seats and using it as an advantage. For this type of seat, the internal pressure pushes the gasket from the downstream seat to the wall of the internal surface of the secondary body and, consequently, the secondary body pushes the seat back to the ball. Therefore,

only a few small particles manage to leave the second sealing zone, by passing through the sealing surface between the sealing seat and the ball. Thus, highly safe sealing is ensured.

In pipeline networks for natural gas, other sealing methods are also used, such as soft sealing. In this case, gaskets made from Viton, NBR (nitrile butadiene rubber), or other materials are able to keep all of the pressure upstream of the internal zone of the ball, without leakages. The problem occurs if a fire develops in the pipeline network, because the soft sealing is destroyed, subjecting the entire system to an unacceptable situation. It is true that gaskets made from Viton, Isolast perfluoroelastomer (FFKM), etc., can resist temperatures of almost 300 °C. For example, Viton can survive up to 3000 h at 232 °C, 1000 h at 260 °C, 240 h at 288 °C, and 48 h at 316 °C [28]; however, there are still risks. Metal–metal sealing is the only method that can be used to stop the spread of fires in pipelines. This is the recommended technical solution to be applied in ball valves used for the transportation of natural gas, which require fire-safe conditions.

3.6. Analysis of Results

A comparison between the present work and other studies performed using CFD methods reveals some similar results, although the investigated ball valves had different designs. For instance, in the simulation performed by Tabrizi A. et al. regarding how cavitation conditions influence the performance of ball valves [6], some similarities with the flow patterns obtained for small opening angles may be noticed, such as the dimensions of the vortices, which are high at small opening angles, decrease when the opening angle increases, and almost completely disappear at full opening. The visualization of the phenomena is in accordance with the decrease in the pressure drop when the valve is opening.

The results obtained in this work for case studies with closure angles of 30°, 45°, 60°, and 70° indicate that the increase in the pressure drop when the valve is closing is produced by the enhancement of the chaotic motion of the fluid. This explains why the flow characteristics of the ball valve cannot be linear or exponential and, therefore, why such types of valves are not recommended to be used as control valves. Additionally, the increase in the rates of the fluctuating velocities of the turbulent flow generates an increasing impact on the seats. The upstream seat is highly exposed to a wide range of excessive kinetic energy that becomes increasingly unsteady stress and, in the long term, will damage the seat if the valve is used in the intermediary opening position. On the other hand, when the valve is fully open, the velocities are minimal, the internal walls of the ball valve have a geometry almost to the same as the geometry of the internal walls of the pipeline and, without obstacles, no significant deviations of the flow occur, and the seats can resist not only the nominal pressure, but also overpressure in both the fully open and fully closed positions.

Therefore, the simulations presented in Sections 3.1–3.5 demonstrate why the ball valve is a shut-off valve that must work only in the fully open and fully closed positions. Additionally, the simulation demonstrates why the metal–metal (MM) sealing with double-piston effect (DPE) seats produces low leakage rates, including for the shut-off position; the pressure field reveals that few gas particles succeed in crossing the upstream sealing zone, and even fewer can cross the downstream sealing zone. In conclusion, the DPE design of sealing seats is very safe and ultimately ensures very low leakage.

4. Hydrostatic Tests

The same DN500 ball valve studied by simulation was investigated by hydrostatic tests to verify whether leakages were really low for this ball valve with MM sealing and a DPE design. The hydrostatic tests represent the classic method to verify the quality of sealing. Water is used to visualize whether there are issues and to avoid explosion of an improperly designed valve. Standards that describe procedures to be used for tests on ball valves—namely, API 6D [19], SR EN 14313 [20], and ISO 5208 [29]—were used.

Firstly, the hydrostatic shell test was performed, with the DN500 valve in the partially open position during the experiments. At the end of the body, the cavity was obturated to allow the transmission of the force generated by the full pressure from the end blanks to the body of the valve. The standards require that the pressure must be 1.5 times higher than the nominal pressure, which was 6.3 MPa for the investigated ball valve, which means an overpressure of 9.45 MPa. The valve must be tested at constant pressure, and the duration of the test must be in accordance with the nominal diameter of the valve. For example, for $DN \leq 100$ mm, the duration of the test should be 2 min; for DN between 150 mm and 250 mm, the duration of the test should be 5 min; for DN between 300 mm and 450 mm, the test duration should be 15 min; and for valves with DN 500 or larger, the test duration should be 30 min.

The next test—the hydrostatic backseat test—was conducted in highly clean conditions, without sealants or lubricants on the ball or on the zone of the seats. The standards stipulate that the test pressure should be 1.1 times higher than the working pressure. For this test, the duration must also be in accordance with the nominal diameter, but the testing period is different from that of the previous test. For the valves with a nominal diameter over 500 mm, which is in the scope of this work, the test duration must be 5 min.

The good quality of the sealing is demonstrated for the valves with soft sealing if there is no visually detectable leakage during the tests. According to the standard ISO 5208:2015 [29], for the valves with PMSS (primary metal–secondary soft) sealing or MM (metal–metal) sealing, the maximum allowable leakage fluid flow rate defines the category of safety to which the valve is supposed to belong. Information extracted from ISO 5208 is presented in Table 1.

The test bench used for tests on the ball valve is presented in Figure 16. The equipment contains a hydraulic clamping system and control-panel-mounted test gauges capable of performing shell tests and seat tests on DN15–DN1000 flanged-end valves, in accordance with international test standards. The pressure used during the tests can be from 1.6 to 42 MPa. The test bench can use water, gas, or oil as the working fluid. The details and the schematic components of the test bench presented in Figure 16 were extracted from the DORY-YFJ-B300 (JWZ-300) equipment manual [30]. In this work, the hydrostatic shell test used water as the fluid, and the hydrostatic backseat tests were performed with air.

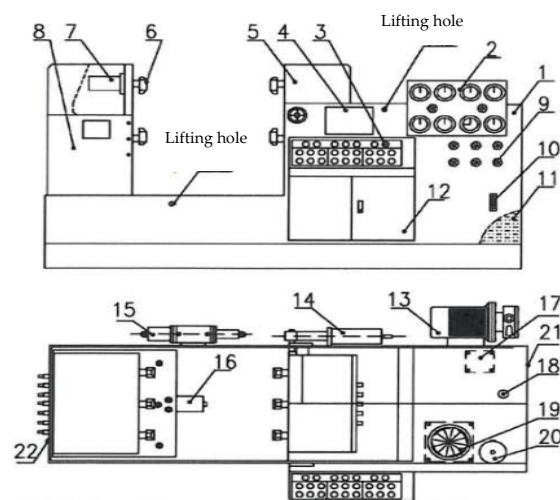


Figure 16. Structural schematic diagram. Components: 1. Hydraulic control station; 2. Panel of pressure gauge; 3. Panel of control button; 4. Pressure checklist; 5. Turning bench; 6. Clamping claws; 7. Clamping oil cylinder; 8. Moving bench; 9. Control valves; 10. Oil volume gauge; 11. Oil tank; 12. Electric box; 13. Low-pressure water supply pump; 14. Turning oil cylinder; 15. High-pressure water supply pump; 16. Moving oil cylinder; 17. Hydraulic and integrated components; 18. Oiling port; 19. Hydraulic motor and oil pump; 20. Pressurizing oil cylinder; 21. Oil draining; 22. Water draining [30].

Table 1. Maximum allowable closure test leakage rate according to API 6D [19].

Test Fluid	Unit Leakage Rates	Rate A	Rate AA	Rate B	Rate C	Rate CC	Rate D	Rate E	Rate EE	Rate F	Rate G
Liquid	mm ³ /s	No visually detectable leakage	0.006 × DN	0.01 × DN	0.03 × DN	0.08 × DN	0.1 × DN	0.3 × DN	0.39 × DN	1 × DN	2 × DN
Gas	Bubbles/s		0.003 × DN	0.0046 × DN	0.0458 × DN	0.3407 × DN	0.4584 × DN	4.5837 × DN	7.1293 × DN	45.837 × DN	91.673 × DN

The maximum allowable leakage fluid flow rate is a requirement stipulated by the beneficiary, and it is essential to achieve it. The results obtained by the hydrostatic shell test with water as the working fluid and are presented in Table 2, along with the results of the hydrostatic backseat tests (also performed with water).

Table 2. Results of hydrostatic tests performed with water as the working fluid.

Test–Fluid Test	Pressure (MPa)	Time (s)	Fluid Flow Rate of Leakage (ml/s)—Required Values	Fluid Flow Rate of Leakage (ml/s)—Result Values
Hydrostatic shell test	94.5	1800	No external leakages	No external leakages
Hydrostatic test of the upstream seat	6.93	300	0.05	0.043
Hydrostatic test of the downstream seat	6.93	300	0.05	0.041

The results obtained with air as the working fluid are presented in Table 3.

Table 3. Results of hydrostatic tests with air as the working fluid.

Test–Fluid Test	Pressure (MPa)	Time (s)	Fluid flow Rate of Leakage (Bubbles/s)—Required Values	Fluid Flow Rate of Leakage (Bubbles/S)—Result Values
Hydrostatic test of the upstream seat—low-pressure air	0.6	300	230	0
Hydrostatic test of the downstream seat—low-pressure air	0.6	300	230	0
Hydrostatic test of the upstream seat—high-pressure air	6.93	300	230	193
Hydrostatic test of the downstream seat—high-pressure air	6.93	300	230	189

The tests performed with water indicated 0.043 mL/s leakage for the upstream seat and 0.41 mL/s for the downstream seat. For DN500, this means that the valve has 43 mm³/s and 41 mm³/s of fluid flow rate for leakage, respectively, and can be classified in safety category D, which accepts up to 0.1 × 500 mm³/s of fluid flow leakage for tests performed with liquids.

For tests performed with air, the limit for category D is 0.4584 × DN500 = 230 bubbles, according to ISO 5208:2008 [29] and API 6D—paragraph 11.4.3 [19]. The hydrostatic testing of the seats with air must be performed at a pressure 10% higher than the nominal pressure. The tests performed according to the recommendations stipulated in the standards indicated that the ball valve with MM sealing and a DPE design has very good performance and can withstand 10% overpressure. The results of the backseat tests with air, presented in Table 3, classify the ball valve in the same safety category (D).

The tests are mandatory for each new valve, designed to meet the special requirements of the beneficiary. If the valve does not pass the tests, another design solution must be identified, and a new valve must be constructed. It is important to point out that to obtain the safety categories AA or B, the seats should be sealed with soft gaskets. The problem with such solutions is that if a fire occurs, soft gaskets are destroyed quickly; therefore, they are not appropriate for natural gas pipelines. In conclusion, the category D identified for the investigated ball valve is accurate enough to allow the product to be used in natural gas pipelines.

5. Conclusions

The design of reliable and safe valves is crucial for the operation and extension of natural gas pipeline networks. In this work, fluid flow simulations for a DN 500 mm

trunnion ball valve were performed for five positions of the ball—from slightly to fully closed—using SolidWorks Flow Simulation 2023. Based on the observation of the pressure fields, the velocity fields, and the trajectories, several conclusions can be put forward.

For partially closed case studies, when the angle between the longitudinal axis of the pipe/ball valve and the longitudinal axis of the ball was 30°, 45°, 60°, or 70°, the increase in the closure angle modified the pressure fields and trajectories significantly. In large-diameter ball valves, vortices have enough space to develop; consequently, their amplitude is larger compared to small and medium-sized valves. Intense turbulence phenomena lead to high levels of unsteady stress on the sealing components and important pressure losses at high closure angles. The results obtained by simulation of a ball valve in intermediary closing positions strengthen the recommendation to construct ball valves merely for shut-on/off applications. This technical requirement is usually based on the difficulties of designing them in such a way as to be used as control valves, providing appropriate fluid flow characteristics. This paper demonstrates that in order to obtain reliability, the shut-on/off operation of large-diameter ball valves is mandatory.

If the ball valve is supposed to operate for a long time interval in an intermediary opening position, the flow pattern should be studied by dynamic simulation to identify the risky areas. Thus, the internal geometry of the ball and of the sealing seats can be configured on a case-by-case basis by the mechanical engineer responsible for their design.

The simulation for the case study with a closure angle of 90° demonstrates the importance of implementing the DPE seat type for good sealing of large-diameter ball valves. Some suppliers use an SPE design for upstream seats, because they are cheaper. Unfortunately, such sealing allows some particles to pass, and without DPE downstream seats, particles of fluid can be released in the pipe, which is unacceptable for natural gas as a fluid.

Ball valves that work with water are exposed to the risk of cavitation and of erosion due to solid particles. Although ball valves working with natural gas are risk-free from this perspective, they are exposed to the risk of fire. To avoid the propagation of fire in the pipeline, the ball valve must be safe enough to shut circulation of the gas for a long period. This work shows that only a few particles succeed in crossing the internal cavity of the principal body; therefore, large trunnion ball valves with an MM DPE design for the seats can be used to isolate the sections of gas pipelines that are on fire and stop propagation in the neighboring sections.

Author Contributions: Conceptualization and methodology, D.P. and L.-I.I.; software, L.-I.I.; validation, formal analysis, investigation, resources, and data curation, L.-I.I. and D.P.; writing—original draft preparation, D.P. and L.-I.I.; visualization, L.-I.I.; supervision and project administration, D.P. All authors have read and agreed to the published version of the manuscript.

Funding: Publication costs were partially covered by “Technical University Gheorghe Asachi of Iasi”.

Institutional Review Board Statement: Not applicable.

Informed Consent Statement: Not applicable.

Data Availability Statement: The data supporting the results reported in the present study will be available upon request from the corresponding author or the first author.

Conflicts of Interest: The authors declare no conflict of interest.

References

1. EUROSTAT. Natural Gas Supply Statistics. Consumption Trends. Available online: https://ec.europa.eu/eurostat/statistics-explained/index.php?title=Natural_gas_supply_statistics#Consumption_trends (accessed on 3 February 2023).
2. ACER. European Union Agency for the Cooperation of Energy Regulators. Available online: <https://www.acer.europa.eu/gas-factsheet> (accessed on 3 February 2023).
3. Market Observatory for Energy, Volume 15, Issue 3, Covering Third Quarter of 2022. Available online: <https://energy.ec.europa.eu/system/files/2023-01/Quarterly%20report%20on%20European%20gas%20markets%20Q3%202022.pdf> (accessed on 3 February 2023).

4. European Commission. REPowerEU: A Plan to Rapidly Reduce Dependence on Russian Fossil Fuels and Fast forward the Green Transition. Available online: https://neighbourhood-enlargement.ec.europa.eu/news/repowereu-plan-rapidly-reduce-dependence-russian-fossil-fuels-and-fast-forward-green-transition-2022-05-18_en (accessed on 3 February 2023).
5. A 350/A 350 M—04; Standard Specification for Carbon and Low-Alloy Steel Forgings, Requiring Notch Toughness Testing for Piping Components. American Society for Testing and Materials: West Conshohocken, PA, USA, 1999.
6. Tabrizi, A.; Asadi, M.; Xie, G.; Lorenzini, G. Computational fluid-dynamics-based analysis of a ball valve performance in the presence of cavitation. *J. Eng. Thermophys.* **2014**, *23*, 27–38. [[CrossRef](#)]
7. Mao, Z.; Yoshida, K.; Kim, J. A micro vertically-allocated SU-8 check valve and its characteristics. *Microsyst. Technol.* **2019**, *25*, 245–255. [[CrossRef](#)]
8. Dumitrache, C.; Hnatiuc, B. Comparative CFD analysis of naval plug valve. *J. Phys.* **2018**, *1122*, 1–49. [[CrossRef](#)]
9. Xu, Y.; Guan, Y.; Liu, Y.; Xuan, L.; Zhang, H.; Xu, C. Structural optimization of downhole float valve via computational fluid dynamics. *Eng. Fail. Anal.* **2014**, *44*, 85–94. [[CrossRef](#)]
10. Žic, E.; Banko, P.; Lešnik, L. Hydraulic analysis of gate valve using computational fluid dynamics (CFD). *Sci. Rev. Eng. Environ. Sci.* **2020**, *29*, 275–288. [[CrossRef](#)]
11. Lin, F.; Schohl, G. CFD Prediction and Validation of Butterfly Valve Hydrodynamic Forces. In Proceedings of the World Water and Environmental Resources Congress 2004, Salt Lake City, UT, USA, 27 June–1 July 2004; p. 232.
12. Jia, M.; Li, Z.; Jia, L.; Liu, J. Structural optimization of V-sector valve cores and adaptability in secondary heating networks. *Flow Meas. Instrum.* **2021**, *81*, 102032. [[CrossRef](#)]
13. Yu, R.; Wu, Y.; Chen, X.; Wu, X. Study on the design of ball valve based on elastic ring valve seat structure and fluid characteristics and fatigue strength. *Flow Meas. Instrum.* **2023**, *89*, 102302. [[CrossRef](#)]
14. Song, X.; Kim, S.; Baek, S.; Park, Y. Structural optimization for ball valve made of CF8M stainless steel. *Trans. Nonferrous Met. Soc. China* **2009**, *19*, 258–261. [[CrossRef](#)]
15. Chern, M.; Wang, C.; Ma, C. Performance test and flow visualization of ball valve. *Exp. Therm. Fluid Sci.* **2007**, *31*, 505–512. [[CrossRef](#)]
16. Cui, B.; Lin, Z.; Zhu, Z.; Wang, H.; Ma, G. Influence of opening and closing process of ball valve on external performance and internal flow characteristics. *Exp. Therm. Fluid Sci.* **2017**, *80*, 193–202. [[CrossRef](#)]
17. Peng, C.; Fischer, F.; Schmitz, K.; Murrenhoff, H. Comparative analysis of leakage calculations for metallic seals of ball-seat valves using the multi-asperity model and the magnification-based model. *Tribol. Int.* **2021**, *163*, 107130. [[CrossRef](#)]
18. Velázquez, J.; González-Arévalo, N.; Díaz-Cruz, M.; Cervantes-Tobón, A.; Herrera-Hernández, H.; Hernández-Sánchez, E. Failure pressure estimation for an aged and corroded oil and gas pipeline: A finite element study. *J. Nat. Gas Sci. Eng.* **2022**, *101*, 10453219. [[CrossRef](#)]
19. API 6D:2014; Specification for Pipeline Valves. American Petroleum Institute: Washington, DC, USA, 2014.
20. ISO 14313:2007; Petroleum and Natural Gas Industries—Pipeline Transportation Systems—Pipeline Valves. ISO: Geneva, Switzerland, 2007.
21. SR EN 3317:2015; Natural Gas. Technical and Quality Conditions. TRANSGAZ: Medias, Romania, 2015.
22. ANRE (Romanian Energy Regulatory Authority). Anexa nr. 5 din Ordinul 62/24.06 2008 Privind Regulamentul de Masurare a Cantitatilor de Gaze Naturale Tranzactionate în România Completata cu Ordinul nr. 2 din 18 Ianuarie 2023 Pentru Modificarea Și Completarea Ordinului Președintelui Autorității Naționale de Reglementare în Domeniul Energiei nr. 89/2018 Privind Aprobarea Normelor Tehnice Pentru Proiectarea, Executarea Și Exploatarea Sistemelor de Alimentare Cu Gaze Naturale. Publicat în MONITORUL OFICIAL nr. 67 din 26 ianuarie 2023. Available online: <https://legislatie.just.ro/Public/DetaliiDocument/264378> (accessed on 4 February 2023).
23. MaxCarbide. Carbide Valve Ball and Seat. Available online: <https://www.maxcarbide.com/products/stellite-alloy-balls-and-valve-seats-blanks> (accessed on 23 January 2023).
24. Hardide Coatings. Tungsten carbide coating for ball valves. *World Pumps* **2009**, *9*, 12.
25. Ivancu, L.; Popescu, D. Design Solutions for Large Size Ball Valves. *Bul. Inst. Politeh. Din Iași* **2022**, *68*, 51–59. [[CrossRef](#)]
26. Dassault Systems. *Technical Reference SolidWorks Flow Simulation 2023*; Dassaults Systems: Waltham, MA, USA, 2023.
27. MyDatabook. Available online: https://www.mydatabook.org/fluid-mechanics/flow-coefficient-opening-and-closure-curves-of-full-bore-ball-valves/#kv_tables (accessed on 28 January 2023).
28. DuPont Dow Elastomers. Viton Selection Guide. Available online: <https://rainierrubber.com/wp-content/uploads/2014/01/Viton-Selection-Guide.pdf> (accessed on 29 December 2022).
29. ISO 5208:2015; Industrial Valves—Pressure Testing of Metallic Valves. ISO: Geneva, Switzerland, 2015.
30. DORY Total Solution for Valve Testing & Grinding; User Manual DORY-YFJ-B300 (JWZ-300); DORY: Zhejiang, China. Available online: <https://globalsupplyline.com.au/wp-content/uploads/2014/09/Valve-Test-Bench.pdf> (accessed on 25 March 2023).

Disclaimer/Publisher’s Note: The statements, opinions and data contained in all publications are solely those of the individual author(s) and contributor(s) and not of MDPI and/or the editor(s). MDPI and/or the editor(s) disclaim responsibility for any injury to people or property resulting from any ideas, methods, instructions or products referred to in the content.